Interoperability between BIM and FEM for vibration-based model updating of a pedestrian bridge

Aliasghar Talebi[1], Francesco Potenza[2#], Vincenzo Gattulli[3]

1. *Ph.D. Student, Department of Structural and Geotechnical Engineering, Sapienza University of Rome, via Eudossiana 18, 00184 Rome, Italy; aliasghar.talebi@uniroma1.it*
2. *Assistant Professor, Department of Engineering and Geology, University G. d'Annunzio of Chieti-Pescara, Viale Pindaro 42, 65127 Pescara, Italy; francesco.potenza@unich.it*
3. *Full Professor, Department of Structural and Geotechnical Engineering, Sapienza University of Rome, via Eudossiana 18, 00184 Rome, Italy; vincenzo.gattulli@uniroma1.it*

\# *Corresponding author: francesco.potenza@unich.it*

Abstract

Finite Element Model (FEM) updating is the procedure of minimizing errors between the experimental measurements and response simulated by FEMs. It can lead to more accurate and representative models useful to perform forecast analysis or detect initial damage thresholds for structures and infrastructure. The paper investigates the potentialities to carry out an automatic model updating through the interoperability between FEMs, Building Information Modeling (BIM), and experimentally vibration-based information. Indeed, these latter possess details and data (geometrical or mechanical) that could be automatically transferred in a numerical environment for structural modeling. The ability of this exchange is assessed by a methodology applied to a pedestrian walkway. The first path utilizes the geometrical data coming from a BIM model of the walkway to achieve three different levels of meshing. Consequently, three accurate finite element modelings have been pursued based on the achieved discretization. For each model, the accuracy and cost analysis has been evaluated considering the minimal distance between the main experimental modal parameters, identified from output-only dynamic tests, and the numerical ones, obtained after manual model updating. ~~Instead~~Additionally, a second path ~~tries~~ attempts to realize an automatic model updating ~~by~~ through a simplified representative numerical system of the walkway implemented in Matlab. To this ~~aim~~end, first,~~ly~~ an opportune algorithm has been developed capable of processing the data and information ~~coming by~~from both BIM and experimental identification ~~has been developed~~. Second~~ly~~, once the numerical model is realized, the potentiality of a modified Particle Swarm Optimization for improving the structural representativeness has been assessed. In particular, the usefulness of this approach could be related to a smart management system of the structures and infrastructure through a corresponding digital twin model.

Keywords: Dynamic Test, Modal Identification, Finite Element Model Updating, Particle Swarm Optimization, Footbridges

1. Introduction

Finite element model updating is commonly used as a procedure aiming to obtain an accurate and realistic structural model based on the information coming from experimental tests [1]. This latterSuch a structural model could be useful also to calibrate simplified analytical models [2], [3], [4] useful to evaluate, with a smaller margin of uncertaintyness, parameters like damping [5] or structural damage [6], [7]. One of the ways to improve the representativeness of a numerical model is through the identification of those parameters that mainly affect the dynamic behavior (such as the elastic modulus in concrete structures) [8], [9]. The unavoidable differences between the characteristics of designed and as-built structures in the corresponding numerical models introduce a certain level of uncertainty. Among the various experimentalVibration-based experimental tests mostly carried out to improve the knowledge of structural behavior, the vibration-based ones are surely widely used by both researchers and practitioners, to improve knowledge of structural behavior. Moreover, as well-known from for at least twenty years, dynamic measurements, acquired in someat selected points of the a structure and induced by ambient vibration (i.e. without the direct quantification of the input), have shown considerable convenience and utility. The reasons are easily understandable: (1) easeiness in the setup implementation and data management, (2) avoiding the use of cumbersome instrumentation (especially related to the machines used for generating input on the structures, such as a hammer or shaker), (3) applicability of different output-only procedures for modal identification (some of which are well-known in the literature). Indeed, related to this last point, since the ambient vibrations are commonly considered as a white noise input, the frequency content of the corresponding output is reasonably associable with the main modal frequencies of the structure. Stochastic Subspace Identification (SSI) [10] and the PolyMAX procedure [11] are two of the most important techniques applied for such purposes. In brief, in the first case, the stochastic state-space models identified directly from measured output-only data can be considered a good representation of a structure subjected to an unknown force modeled as white noise. In the second case, the estimation of the modal parameters is pursued by processing the measured ouput in an opportune way the measured output. Sometimes, also, the SSI has been also applied using seismically-induced responses that, from a sideon one hand, could be useful to increase the level of the recorded amplitudes (achieving a modal signature even when low-sensitivity sensors are used) but, from on the another sidehand, the measurements could have a high non-stationary behavior producing an approximate identification. In the literature, among the various open-source softwares, developed for dynamic identification, PyOMA is surely worthy to beof being mentioned [12]. In suchThe application have been implemented thehas been used by researchers, engineers and practitioners to implement the most common procedures dedicatd to theof output-only Operational Modal Analysis in an easialy manageable by researchers, engineers and practitionersway. Beyond daily dynamic tests, it should also be mentioned, that also long-term and continuous Structural Health Monitoring (SHM) systems, using data-driven procedures, can provide further information on concerning the dependence of the structural behavior by environmental induced frequency dependence [13] (temperature and humidity) which can be related to structural variation in behavior or insights in the modification during seismically-induced response due to damage evolution using also data-driven procedure [14].

Footbridges are surely among the structures most, widely analyzed worldwide through using the information coming from dynamic tests. They are different from other bridges (viaducts, railways, or highway bridges), especially relating theirin regard to the need to take into account their interaction with pedestrian traffic (i.e. human-induced vibrations) that cannot be neglected. In this sense, aAn interesting case was the London Millennium footbridge that, during the its opening day, showed unexpected lateral movements when pedestrians crossed the footbridge [15]. Moreover, in order to prevent these anomalies aA possible retrofit was designed, aiming at to control these anomalous vibrations control using both viscous and tuned mass dampers were also designed. Modern walkways are in general very slender structures ~~and so they could~~that can be highly affected by human-induced vibrations. Interesting cases can be found in [16]–[19]. In [16] is illustrated one of the first experimental activities to opportunely minimize the differences between designed and as-built structure characteristics~~ is illustrated~~. In this case, ~~the~~ vibration tests were carried out using both artificial (electrodynamic shaker) and ambient vibration excitations. The identification results were very useful to calibrate the stiffnesses of girder end supports in the longitudinal direction and the bending stiffness of inclined columns. In [17] the methodology proposed by recent European guidelines (HiVoSS and French guidelines Setra) is evaluated to estimate the effects of ~~the~~ serviceability vibrations. based on simplified load models representative of crowd-induced loading. Eight slender footbridges ~~have been~~were selected as testbeds. ~~for which have been found i~~Inevitable uncertainties were found between the modal characteristics predicted by numerical models and the ones identified in situ. The authors recommend the use of a modified load model to consider such uncertainties. Other cases are illustrated in [20]–[22]. They are focused on the effectiveness of using updated numerical models to assess both serviceability vibrations and the performance of devices for vibration control. An example of an SHM system implemented in a footbridge is reported in [23]. In the first phase, the application of an automated operational modal procedure on the recorded data showed a significant nonlinear effect on the modal features due to environmental and operational factors like temperature and pedestrian traffic. Subsequently, such behavior ~~has been~~was removed by applying the linear Principal Component Analysis. Moreover, in this case, the updated numerical model ~~has been~~was used as a basis to simulate plausible damage scenarios.

Recently, Building Information Modeling (BIM) has received great attention from researchers involved in the fields of Structural Health Monitoring, Maintenance, and Design support [24], [25]. In particular, the BIM model could be useful to quickly and automatically visualize possible negative trends related to structural behavior. It can constitute an effective tool useful to provide different services or forecasting analysis, ~~like~~ for example, such as the structural ~~one~~analysis~~,~~ usually performed by dedicated Finite Element softwares. Today, the lack of interoperability [26] of the BIM models (e.g. automatically switching between BIM and FEM) ~~is~~ remains an open issue~~ yet~~. Integration of the BIM model and information coming ~~by~~ from vibrational measurements (daily experimental tests or continuous monitoring) could help in the overall management of ~~the~~ a building [27]. Moreover, the correct representation of the geometry~~,~~ that can be achieved by the BIM model~~,~~ is certainly very useful for addressing an optimal calibration of a numerical model.

In this ~~sense~~direction, this paper aims to propose a possible path ~~to~~ for obtaining a complete automatic exchange between BIM and FEM. In particular, the chain BIM-FEM-model updating is pursued using a procedure implementable in numerical software such as Matlab. The paper is organized as follows. Section 2 briefly presents the methodology whose performance will be evaluated through a case study (a footbridge located in the historic center of Rome). In Section 3 the geometric and structural characteristics of the walkway and the implementation of the BIM model are described. Section 4 illustrates the results of the dynamic tests and the subsequent modal identification. The last section shows how the manual model updating is performed, driven both by~~ both~~ refined geometrical information coming from BIM and modal features identified through experimental data ~~of~~ from three different modeling approaches (using 1D, 2D, and 3D finite elements)~~ is performed~~. Finally, the ability of a Modified Particle Swarm Optimization for automated model updating has been tested using this case study. In this last procedure, both the FE model and algorithm have been developed in Matlab.

2. BIM-FEM Methodology

In this section, an overall proposed methodology ~~proposed to go forward with possible~~to completely automat~~ion related to the~~e interoperab~~il~~ility ~~between~~ BIM-FEM-model updating is presented. The procedure is shown in Figure 1. The first step regards the in-situ surveys that, in general, could be performed by a Terrestrial Laser Scanner. This is a fundamental action to define the geometric configuration with a low level of uncertainty. Subsequently, the coordinates of the points cloud will constitute a reference base on which to build ~~built~~ a corresponding as-built BIM. This latter will be the starting point for implementing both refined (using commercial applications/software) and simplified FEM models. Through the simplified approach it is possible to ~~follow~~ realize an automated model updating based on ~~the~~ information that could come either from daily dynamic tests or a long-term vibration-based SHM system.

~~In~~ Along this path, among the procedures usable for searching the optimal structural parameters (e.g. stiffness and mass), the metaheuristic optimization algorithms constitute a ~~good chance~~promising option. They aim to find the minimizat~~z~~ion or maximization of a problem. Such procedures are grouped based on their characteristics and the target to be reached. A first subdivision can be done in gradient-based and population-based algorithms. The first ones use derivative information, while the second ones exploit multiple agents trac~~e~~ing different trajectories. In this last grouping a well-known example is given by the Particle Swarm Optimization (PSO, [28]). Such a procedure ~~well~~ fits well with researching the optimal ~~research of the~~ structural parameters, since often they have a stochastic nature. Some examples on the use of the ~~the~~ optimization algorithms can be found in [29], [30], [31]. Instead, the refined FEM models can be improved by ~~the~~ so-called manual model updating that consists ~~of the~~in tuning ~~of some~~ selected parameters to minimize ~~some~~ certain predefined objective functions. It is evident that the whole process could require not only ~~a~~ notable computational time, but also technical supervision. The phases~~,~~ contained within the dashed box in Figure 1 are the ones more easily automatable, for which ~~is minimal~~ the need for human-based supervision is minimal. ~~In the following will be deepened~~ T~~t~~he activities inside the green and blue boxes will be addressed in the following.

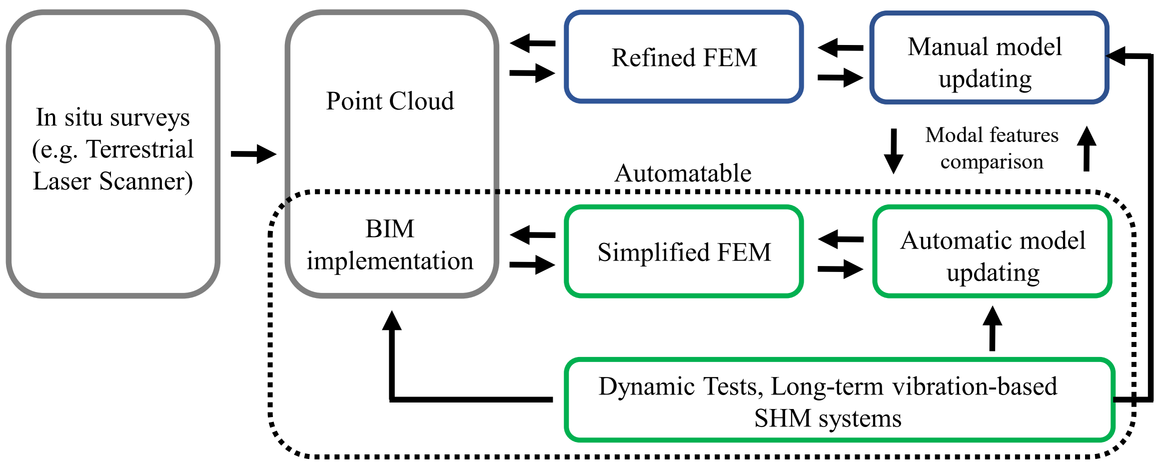

Figure 1. Flowchart related to the exchange/interoperability BIM-FEM-model updating.

3. Pedestrian walkway characteristics

Annibaldi bridge is a pedestrian walkway located in Rome close to the Faculty of Engineering of the University of Rome – La Sapienza. It was built to overpass the avenue "*via degli Annibaldi*" linking together the streets "*via Vittorio da Feltre*" and "*via del Fagutale*" (Figure 2a-c). Crossing the pedestrian walkway provides an opportunity to ~~is possible to~~ admire the majesty of the Colosseum and, for this reason, it is very frequented by tourists (Figure 2a).

The structural conceptual scheme of this footbridge is represented by a simply supported beam. Its total length and width are 20.5 m and 4.0 m, respectively. ~~By~~ From the lateral view (Figure 2a,d) ~~it is possible to visualize~~the walkway presents ~~–~~a longitudinal slight arch shape with~~, approximately,~~ a curvature radius approximately equal to 123 m.

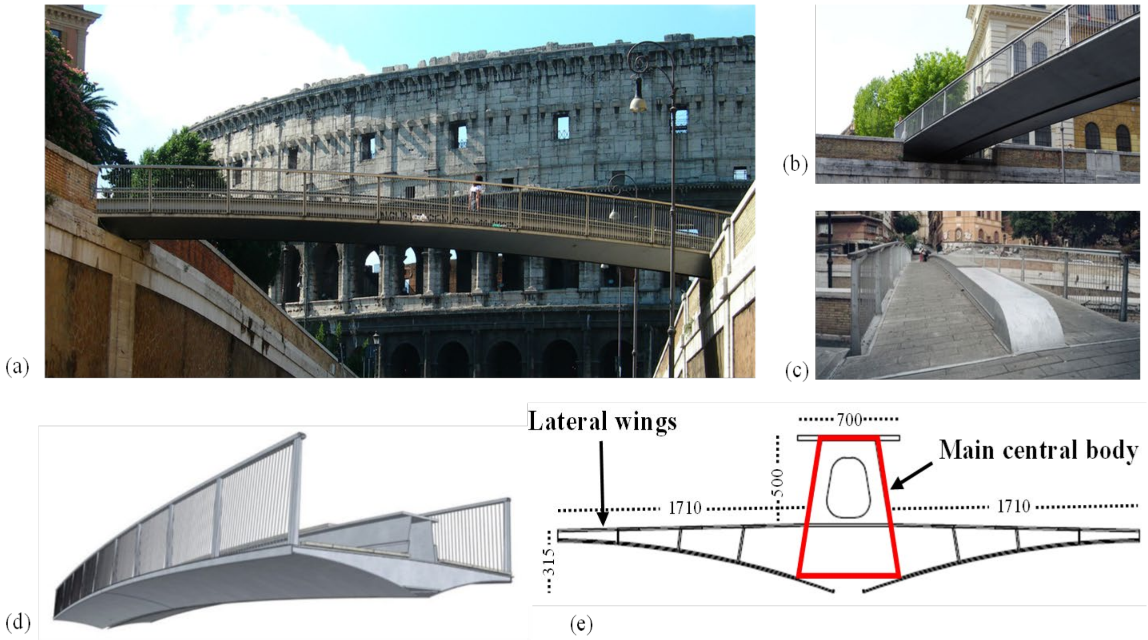

Figure 2. Photos of the Annibaldi pedestrian walkway: (a) longitudinal, (b) from below, and (c) lateral view. (d) 3D view of the BIM model. (e) transversal section scheme (measures in mm).

The elements, constituting the structural part, have been formed of a steel material (Fe510) while the foundations have been made using reinforced concrete (Rbk 300, FeB44k improved adherence). The transversal section is, substantially, composed by three elements (Figure 2e). The main central body is a box girder used as longitudinal beam. Thin steel sheets are assembled in a way to form a trapezoidal shape (highlighted in red in Figure 2e). These sheets have a small thickness (8 mm) and so, to avoid possible buckling phenomena, vertical stiffening plates along the whole longitudinal length (each 2 m) have been inserted. The other two important parts of the transversal section are constituted by the lateral wings (Figure 2e) showing an arch-shaped with a small thickness (7 mm). Therefore, transversal cantilevered elements are linked in both lateral surfaces of the main central body and the lower closure plate of the lateral wings (each 2 m). Moreover, as further stiffening, on the lower plate, longitudinal elements with a *C*-shaped transversal section, three for each side and one for closure have been welded.

From the view of Figure 2a, it may seem that the pedestrian walkway has a skew configuration. However, as is visible in Figure 3a, the two end supports are perpendicular to the longitudinal axis and make the footbridge perfectly symmetric. In Figure 3 the exploded view of the BIM model shows all the elements composing the walkway. In Figure 3b a perspective frontal view of the BIM model that exposes the three main structural parts is displayed: the main central beam, lateral wings, and transversal and longitudinal stiffening.

`

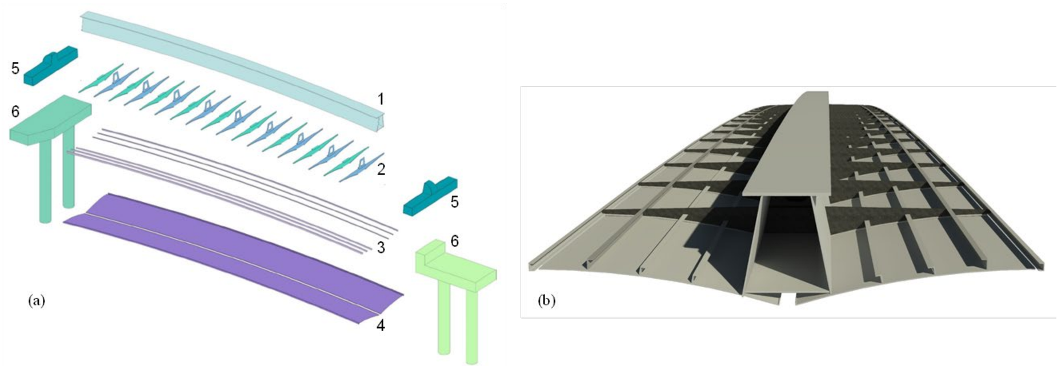

Figure 3. (a) Highlights of all elements making up the walkway: (1) main central body, (2) trans-versal and (3) longitudinal stiffening, (4) lower closure plates, (5) ending elements, (6) supports and foundations. (b) Perspective frontal view of the BIM model.

4. Experimental dynamic tests and modal identification

Dynamics tests have been conducted on two different days: 6 and 18 June 2019. The experimental setup was composed of the following instrumentation:

1. Acquisition system: LMS SCADAS XS and Smart Scope (Figure 4a-b).
2. 6 Piezoelectric accelerometers uniaxial (Figure 4c).
3. Complementary instrumentations (coaxial cables, connections).

LMS SCADAS XS is the core of the data acquisition system and thanks to its ease of portability, it is efficient to maximize dynamic testing performance and suitable for both field and laboratory tests. The main features to be highlighted are the following: (1) the board, illustrated in Figure 4b, can be contained in one hand and it is provided with a built-in battery; (2) it can have three different modes of operation: wi-fi (connected to Smart Scope), standalone and Front-end (connected to the software Simcenter Testlab); (3) it can support 12 analog channels. The Smart Scope is substantially a tablet on which the user can set up, control, and manage the measurement template and also carry out online data processing. The most relevant parameters to be set up are sensor name, point ID and point direction, typology of the physic quantity to be recorded, unit of measure, sensitivity, and acquisition sample rate.

The piezoelectric accelerometers are one of the most used tools by a lot of researchers and

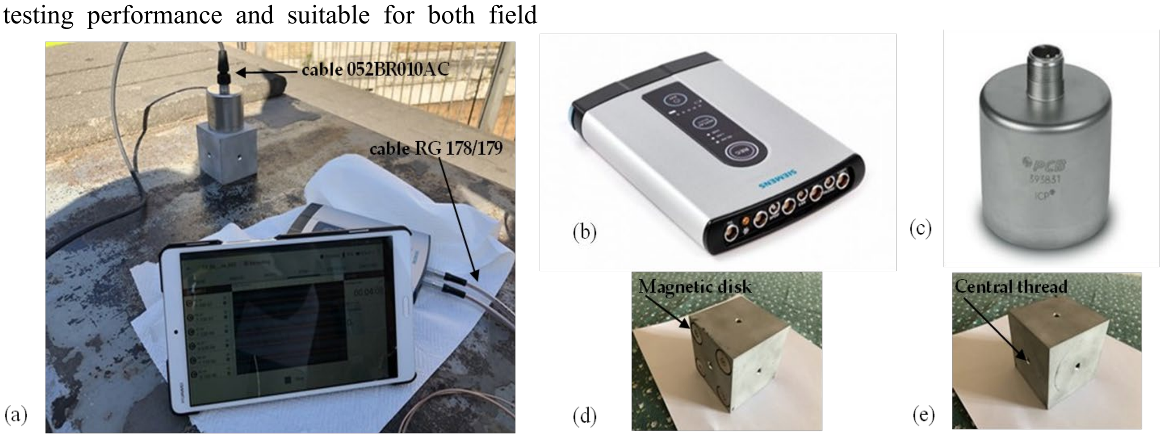

Figure 4. Instrumentation of the experimental setups: (a) acquisition system (LMS SCADAS XS and LMS Smart Scope), (b) LMS SCADAS XS, (c) piezoelectric accelerometer (model 393B31), (d) and (e) connections views

practitioners operating in the civil engineering field. It shows good performance in capturing and providing structural information even when very low amplitude level vibrations are measured. The model utilized in the dynamic tests, PCB 393B31, has an ICP technology that requires only an inexpensive, constant-current signal conditioner to operate. Its main characteristics are reported in Table 1.

Table 1. Features of the 393B31 (PCB) piezoelectric accelerometer

Sensitivity (±5%)	10.0 V/g
Measurement range	0.5 g pk
Frequency range (±5%)	0.1 to 200 Hz
Resonant frequency	≥ 700 Hz
Broadband resolution	0.000001 g RMS
Non-linearity	≤ 1%
Transverse sensitivity	≤ 1%

The complementary instrumentation is composed, mainly of three different typologies of coaxial cables needed for both transmissions of the measured data and power supply. In particular, the coaxial cable RG 178/179 has to be linked to the board LMS SCADAS and the custom-cable 052BR010AC. The other free end of this latter cable has to link connected to the piezoelectric sensor. A third cable (coaxial cable RG58) is used only as an extension function inserting it between the two previous cables. Moreover, to obtain a reliable link between the sensor and structure a customized aluminum cube with a central thread in each face to connect the accelerometric sensor (Figures 4d,e) has been used. Furthermore, on one face of the cube four magnetic plates (disks) for a rapid and easy connection with the steel structure have been inserted (Figure 4d).

In Figure 5 the experimental layouts implemented during the dynamic tests on the 6 and 18 June 2019 have been reported. Six sensors placed at a distance of one-quarter, half, and three-quarters of the total length (three in each lateral edge (Figure 4a)) have been used. In the other setup illustrated in Figure 5b, three sensors have been positioned in the central longitudinal line while the other three have been collocated laterally along via the Cavour side. On 18 June 2019, both experimental layouts have been implemented. Further details of the tests carried out on both days are reported in Table 2. It is worth to notice, that the sample frequencies for the tests carried out on 6 and 18 June were 100 Hz and 200 Hz, respectively. There is no substantial motivation for such a choice, moreover, it does not produce particular differences in the modal identification process. The first setup (Figure 5a) has been designed to observe and identify symmetric, anti-symmetric, and torsional modes. On the other hand, the second one (Figure 5b) has been thought to better detect

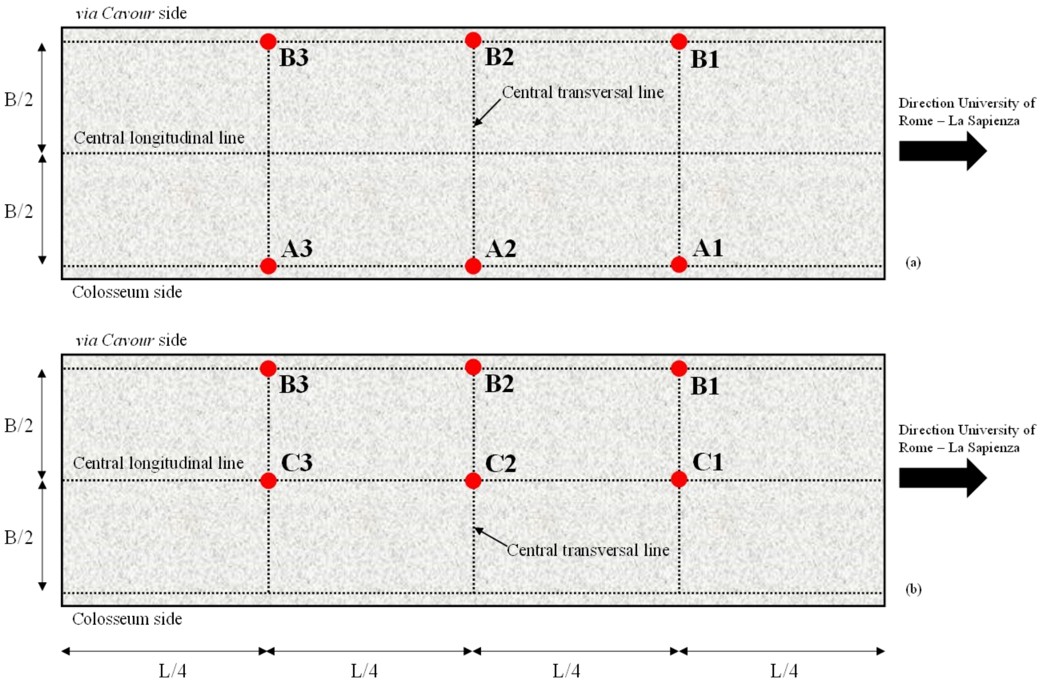

Figure 5. Experimental setups were implemented for the dynamic tests of 6 (a) and 18 June 2019 (a),(b).

the symmetric and anti-symmetric modes concerning the torsional ones. Indeed, the frequencies associated with the torsional modes should not appear (or show a very low amplitude) in the Power Spectral Densities (PSDs) related to the recorded measurement by the sensors located in the central longitudinal line (C1, C2, and C3). It is important to highlight that all recorded accelerations (in all setups) are in the vertical direction because the main modes involved in the dynamic response (visualized by a preliminary finite element model) show an important mass participation ratio in such direction. In Figure 6 the time histories acquired by the second test carried out on 18 June 2019 are reported.

Table 2. Main features of the experimental layouts and tests carried out on 6 and 18 June 2019

Date	Type of input	Test length [min]	Sampling rate [Hz]	Experimental Layout
6th June 2019	Ambiental vibrations	15	100	Figure 5a
18th June 2019 (first test)	Ambiental vibrations	15	200	Figure 5a
18th June 2019 (second test)	Ambiental vibrations	15	200	Figure 5b
18th June 2019 (third test)	Ambiental vibrations	30	200	Figure 5a

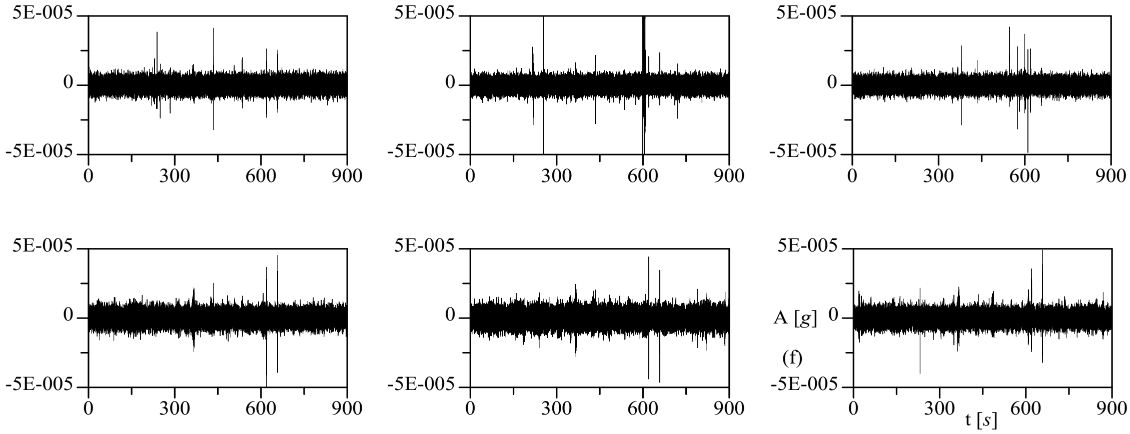

Figure 6. Time histories were acquired during the second test on 18 June 2019.

The graphs related to the accelerations located in the longitudinal lines, central (C1-C3) and lateral (B1-B3), have been inserted in Figure 6a-c and Figure 6d-f, respectively. The registrations show the typical measurement of a structural response subjected to ambient vibrations. Moreover, probably due to the high stiffness of the structure it is possible to observe a very low amplitude level for all measurements in all tests. Indeed, their standard deviations are all largely below 2.5 × 10e-5 g. In the time histories, it is visible the presence of a very low number of spikes presumably due to the passage of some people who have been permitted to cross the walkway during the tests. In Figure 7 the PSDs corresponding to the measurements of the second and third tests carried out on 18 June 2019 have been displayed. The graphs illustrate the PSDs of the measurements corresponding to the transversal lines placed at a quarter (C1-B1 and A1-B1), half (C2-B2 and A2-B2), and three-quarter (C3-B3 and A3-B3) of the whole length. Looking at the frequencies of Figure 7a-c (second test), the one that shows the largest contribution is collocated at 11.410 Hz. It is, most likely, associated with an anti-symmetric mode because it disappears in the PSDs of the sensors placed in the central transversal line (Figure 7b). Figure 7a-c show other two relevant peaks (even if with small amplitude) that are placed at 9.178 Hz and 14.541 Hz. Moreover, they are slightly viewable only in the measurements of the sensors placed on the lateral line (B1-B3) and so, for this reason, they could be associated with torsional modes. The frequency of 4.456 Hz is detectable only in the PSDs related to the sensors C1 and B1 (Figure 7b) probably due to both low amplitude and low participation of such mode in the dynamic response. The same observations can be found for the frequencies that came out processing the registrations of the third test (Figure 7d-f). Indeed, the frequency that shows the highest peak is located at 11.432 Hz as observed in the previous test. In this test, the vibrational amplitude has been higher compared to the previous one. The peaks that could be associated with the structural modes are easier to identify. The frequencies 9.145 Hz and 14.430 Hz are very close to the ones found in the second test (9.178 Hz and 14.541 Hz) that were been previously related to the torsional modes. Finally, especially in the case of the PSDs of recorded measurements by the sensors placed in the central transversal line (A2 and B2 in Figure 7e), the peck in the corresponding frequency of 4.580 Hz is well visible and it is present in both acquisitions (A2 and B2). For this reason, it could be associated with the first symmetric mode. The skewed shapes of all PSDs depicted in Figure 7 (with a high content towards the low frequencies) are due to the presence of strong wind during the two days of the experimental campaign.

Further processing of the acquired data has been pursued through two well-known identification procedures: SSI [10] and PolyMAX [11]. The first performed by MACEC [32] and the second

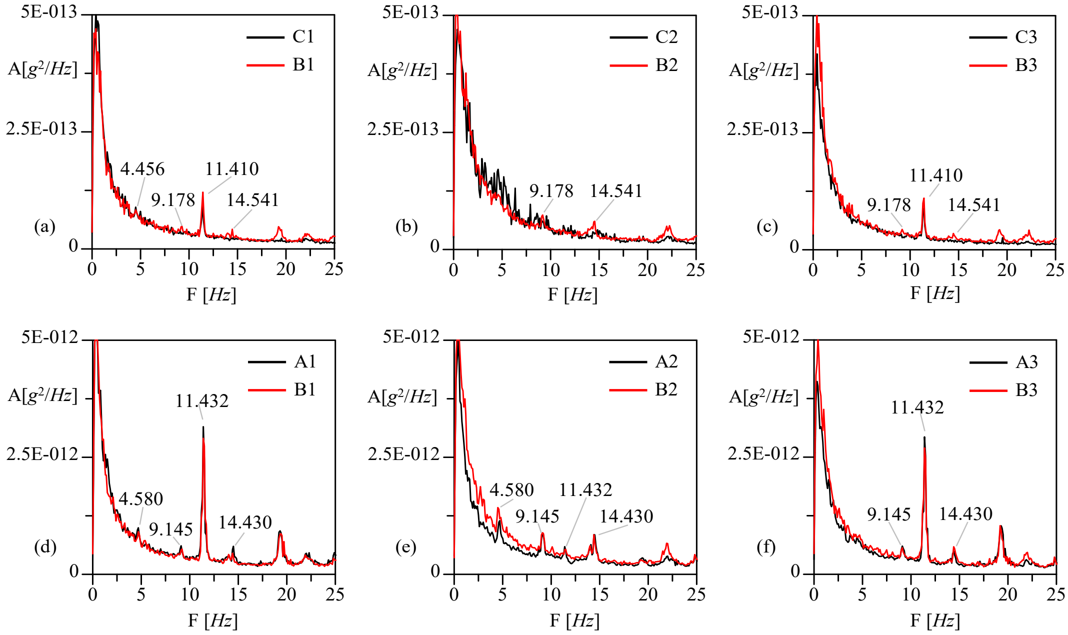

Figure 7. PSDs calculated for the accelerations recorded during the second (a)-(c) and third (d)-(f) tests carried out on 18 June 2019.

one by Simcenter Testlab [33]. In Figure 8 the stability diagram obtained through the PolyMAX procedure analyzing the data recorded during the third test on 18 June, 2019 is illustrated. This graph is clear and the frequencies associable with the structural modes are well-recognizable at 4.580 Hz, 9.145 Hz, 11.432 Hz, and 14.430 Hz. Even in Figure 9, the stability diagram by the SSI algorithm applied to the same measurements is reported. In this case, as in the previous one, the stability diagram doesn't show critical zones and so the interpretation of the frequencies seems to be quite easy. Indeed, the ones associable with structural modes, are the following: 4.580 Hz, 9.145 Hz, 11.432 Hz, and 14.430 Hz which are the same as shown in the PSDs.

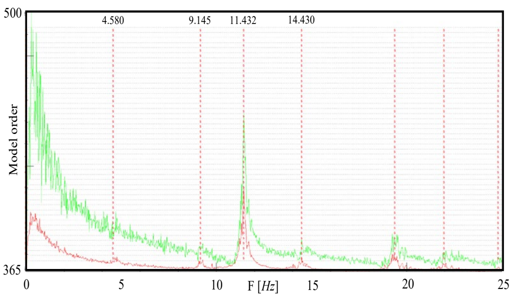

Figure 8. The stability diagram was obtained using the PolyMax procedure. Third test on 18 June 2019. In background: Auto Power sum (green), single Auto Power (red).

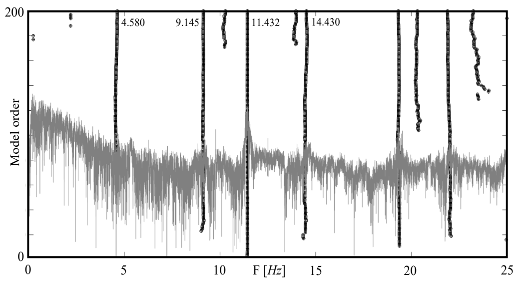

Figure 9. The stability diagram was obtained using the SSI procedure. Third test on 18 June 2019. In background: the Power Spectral Densities.

To the corresponding frequencies can be associated with the modal shapes. In Figure 10 the mode shapes related to the PolyMAX procedure in their perspective view are reported. The first one shows symmetric deformation while the second and third have a torsional shape. The third appears in a flexural and antisymmetric configuration. In this case, critical issues due to the identification of the phase have been found in the external sensors (one and three-quarters of the length). The same modal shapes have been found using the SSI procedure illustrated in Figure 11. Indeed, even in this case, the first one shows a symmetric configuration while the second and fourth have a torsional one.

Table 3. Mean and variance of the frequencies identified by PolyMax and SSI procedure

Mode	PolyMax		SSI	
	Mean [*Hz*]	Variance [Hz^2]	Mean [*Hz*]	Variance [Hz^2]
1	4.562	0.005	4.727	0.016
2	9.156	0.002	9.100	0.008
3	11.463	0.003	11.431	0.002
4	14.516	0.006	14.445	0.014

Table 4. Mean and variance of the damping ratios identified by PolyMax and SSI procedure

Mode	PolyMax		SSI	
	Mean [*Hz*]	Variance [Hz^2]	Mean [*Hz*]	Variance [Hz^2]
1	1.395	0.804	3.465	2.799
2	0.878	0.030	2.127	1.442
3	1.110	0.052	0.961	0.031
4	1.610	0.080	1.821	0.255

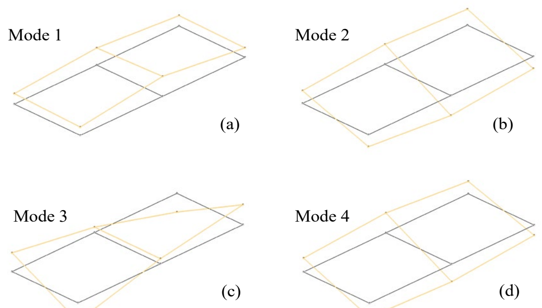

Figure 10. Modal shapes were obtained through the procedure PolyMax (Figure 8).

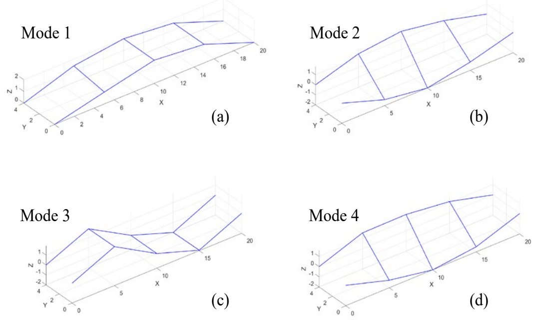

Figure 11. Modal shapes were obtained through the procedure SSI (Figure 9).

Moreover, the identification of the third modal shape results probably correct since it presents a perfect antisymmetric deformation. In Table 3 and Table 4 the mean and variance values for both frequencies and damping ratios identified through the data processing of the measurements obtained by all four tests are reported. The frequencies identified using both procedures are very close to each other, and the variances are very low for all modes, especially in the case of the PolyMAX algorithm. Instead, a higher variability has been found in the identification of the damping. As well-known, this parameter is very difficult to be evaluated but, in any case, the ones obtained through PolyMAX seem to be reasonable for steel structures and possess (on average) a lower variance with respect to the ones found with SSI.

5. Structural Modeling

In this section, the implementation of different typologies of Annibaldi bridge modeling using the information coming from a BIM model is presented.

5.1 Integration of BIM and FE models

FE modeling and its subsequent updating have been pursued by two approaches: (1) manual model updating and (2) automated model updating using Particle Swarm Optimization (PSO). For the data transfer of BIM and FEM, two different processes have been used (Figure 12).
The choice of a suitable finite element model, representative of the structural behavior, depends also on the ability to discretize the geometry of the structure. A BIM model provides a highly detailed 3D model with the information and

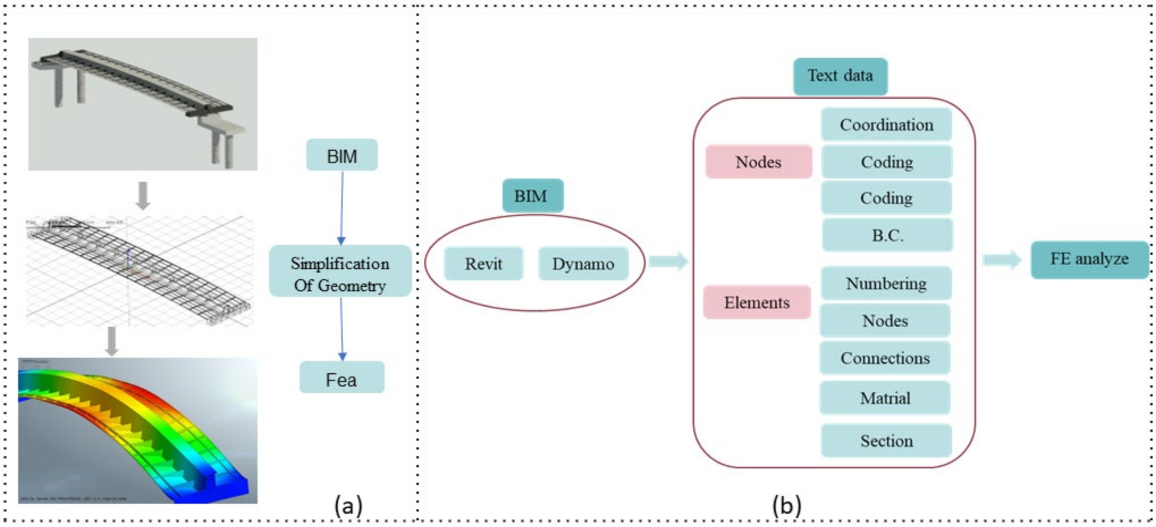

Figure 12. (a) Transferring data from BIM to FE software for manual updating (geometry-only). (b) Process of data exchange from BIM to Matlab algorithm for FE modeling and model updating.

characteristics of elements that could change throughout the life of a structure (e.g. parameters of the materials, size of the corroded areas or position of the boundary conditions).

The interoperability between different aspects related to the management of a building or infrastructure (structural analysis, monitoring, or inspection) is important to reduce the time needed to carry out interventions aiming at structural health. The walkway BIM has been modeled in Revit (Figure 13a), which is one of the most powerful tools for implementing BIM. In the first approach (Figure 12a) only the geometry data have been transferred from BIM to FE. This data has been exchanged by a DXF (Data Exchange Format) file. Midas Civil and Midas FEA NX have been used for structural modeling (Figure 13b-c).

The idealization process of a structural model is an important step that aims to reduce the time and complexity of the solution. However, the BIM model provides both detailed geometric information and element properties, increasing (sometimes excessively) the Degrees of Freedom (DoFs) of the final numerical model. Consequently, the analysis costs due to the

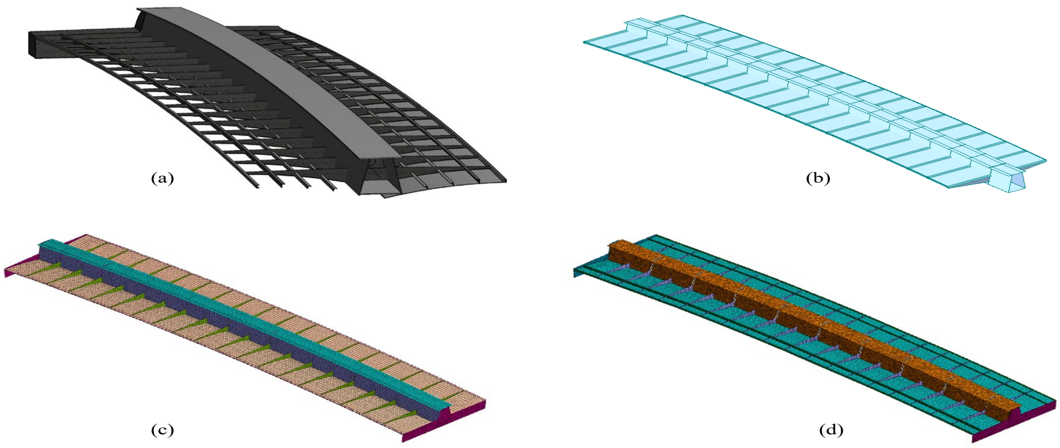

Figure 13. Walkway Annibaldi: BIM model (a) and finite element numerical models: 1 (b), 2 (c), and 3 (d).

Table 5. Models' characteristics and analysis of computational time

Model	Element type	Number of nodes	Number of elements	Degrees of freedom	Average analysis time [s]
1	Beam and Plate	63	131 Beam, 36 Plate	336	0.83
2	Plate	16,971	23,347	101,826	17.50
3	Solid	31,364	67,260	145,863	28.89

enormous amount of data or complexity of geometry could raise too. From this point of view, is always advisable to carry out a cost-benefit analysis to choose the most suitable model.

Here, three different typologies of models have been created to represent the dynamic behavior of the Annibaldi walkway: models 1, 2, and 3 (Figure 13b-d). Model 1 (Figure 13a) has been built through Midas Civil using predominantly one-dimensional elements (beams with two nodes, 6 DoFs for each node). Such elements, in this model, have been inserted to model the main longitudinal beam and the transversal ones (i.e. the elements mainly involved in the dynamic response). Instead, plates or 2D elements have been used to represent the deck and impose permanent loads. However, these plates considering their small thickness, compared to the main beam do not have a notable impact on the global natural modes. Their absence induces the model to show some transversal bending modes in the main beam which are not in line with the experimental results. Therefore, they became very important to correctly model the dynamic behavior and to manage the process of model updating. The other two models, 2 and 3 (Figure 13c,d)), have been implemented in Midas FEA NX through the plate and solid elements, respectively. The first one (model 1) has been highly simplified. Indeed, the walkway has been modeled using a central beam and transversal elements. Models 2 and 3 have a higher level of geometric detail. For all three models, the node coordinates have been selected from the information coming from the BIM model. In Table 5 the main model characteristics have been reported. Looking at these parameters is quite evident a huge difference between the first model (1) and the other two (2 and 3) in terms of DoFs and average analysis time. A better description of the results in terms of deformations and tensions (that could be visualized by models 2 and 3) but inevitably, needs to increase the computational time.

The second approach of modeling has been pursued to go towards automated model updating. In this case, another modality for exchanging data from BIM to FEM will be followed.

The first process transfers the geometry as points defining nodes and curves to form the edges. Subsequently, they are used to generate models 1, 2, and 3 (Figure 12a). On the other hand, for the second approach, which aims to test an optimization-based model updating, a FE algorithm for modal analysis has been implemented in Matlab. The m-file code performs a modal analysis based on the stiffness and mass matrices. These matrices are generated by the FE method using geometry, material properties, and boundary condition. Besides the initial modal analysis (initial FE model), the generated stiffness and mass matrices are used as input for the further model updating process. The model developed in Matlab will be constituted by beam elements in 3D space. The input data for the algorithm are categorized as nodes and elements that can be read from text data or excel. The geometry has been defined through the nodes coming by BIM. To each of these are assigned both code and coordinates. Subsequently, such nodes are connected by elements. Moreover, all elements will be also provided with the section and material properties. They are also coded to be recognized (Figure 12b). Boundary conditions are defined in the corresponding nodes with 0 and 1 for free and fixed restrained DoFs, respectively. These latter are not variable in this model updating. In the automated model, the boundary conditions configuration which was obtained in the manual model updating will be used.

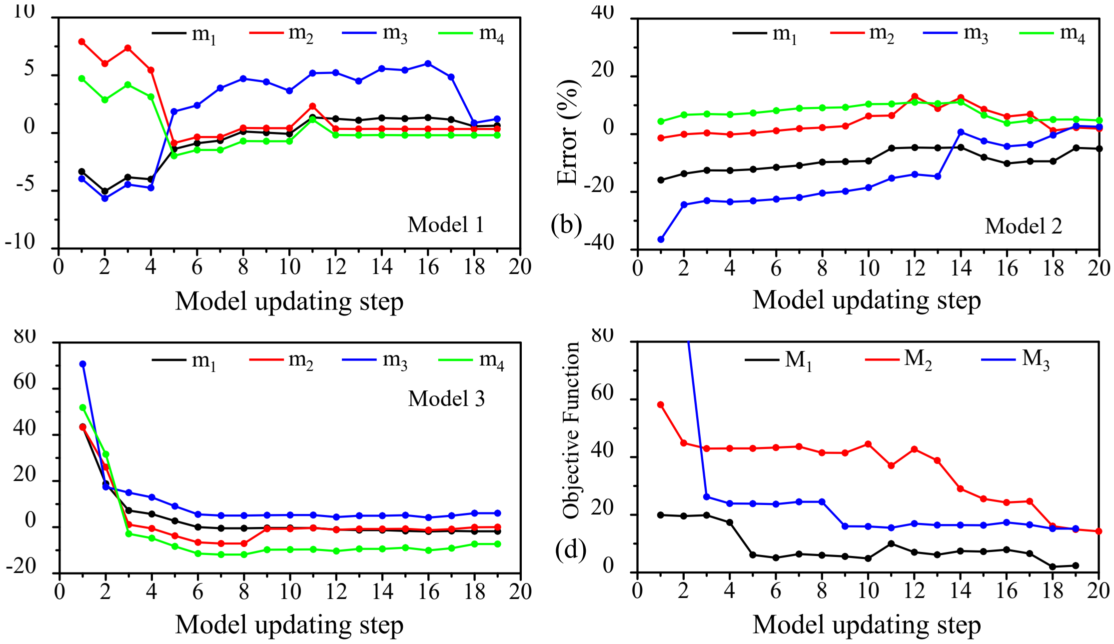

Figure 14. Manual Model Updating: 1 (a), 2 (b), and 3 (c) model. (d) Variation of the objective function for each model (in the graphs, m is for the *i*th mode while M is the model).

5.2 Manual Model Updating

After creating the three FE models based on geometry from BIM, a procedure of manual model updating has been pursued. It aims to find the optimal model characteristics and configurations such that the numerical modal parameters (frequencies and modal shapes), mainly involved in the dynamic response, are in good agreement with the experimentally identified ones. For all models, the following characteristics have been varied:

1. Boundaries Conditions (BC);
2. Elasticity modulus (E);
3. Dead Load (DL, i.e. mass variation);

The objective function *F*, selected to obtain a reasonable improvement, is given by the following expression:

$$F(BC,E,DL) = min\left(\sum_{i=1}^{4}\left|\frac{f_i^{exp} - f_i^{num}}{f_i^{num}}\right|\right) \quad (1)$$

where *F* and f_i^{num} (*i*th numerical frequency) depend on Boundaries Conditions, Elasticity modulus, and Dead Load while f_i^{exp} is the *i*th experimental modal frequency. It is right to highlight that the variation of the Dead Load, substantially, means a mass change. In Figure 14a-c the results of the model updating for each model have been illustrated. In particular, the trend of the percentage variation, for the first four modes, varying characteristics and configurations, is shown. In the ordinate, the percentage of error between experimental and numerical evidence is reported.
In the graphs of Figure 14a-c, the abscissas are referred to the different modeling configurations obtained by varying the features previously described (i.e. boundaries conditions, elasticity modulus, dead load). In Figure 14d the behavior of the objective function for each model is illustrated. For models 2 and 3, the optimal configurations (i.e. minimum value of the objective function) are found in the 20th and 19th step, respectively, while for model 1 it is in the penultimate configuration (18th). In any case, in this latter situation, the difference between the value assumed in the last and penultimate step is negligible.
Moreover, it is right to observe that the best updating is achieved for model 1. Some

observations are the following:

1. there is no a priori rule useful to determine the most influential parameters in the model updating procedure. In any way, is important to detect, through trial and error, the features most sensible to the modal variations;
2. usually, the initial modal difference can be positive or negative (as shown in Figure 14a where is found an initial negative difference for the first and third mode while positive for the second and fourth). For this reason, the improvements (reduction of the difference between experimental and numerical frequencies) have to be pursued operating, at least, on two parameters (e.g. varying elastic modulus and boundary conditions);
3. even if, the initial difference, in some cases, is very high (Figure 14c), an opportune selection of the parameters can provide a final result very close to the desired values.

In Table 6 the comparison between experimental and numerical frequencies is reported (these latter are in correspondence with the last configuration). For all models, a good agreement, especially for the first two modes is found. Indeed, the percentage error is on average widely below 5% (except for the 3rd mode in models 2 and 3 and the 4th mode in model 3). Moreover, the average errors for each model are the following: 0.600 % (Model 1), 3.565 % (Model 2), and 3.863 % (Model 3).

Table 6. Comparison between experimental and numerical frequencies (last step)

Modes	Exp. fr. [*Hz*]	Model 1D		Model 2D		Model 3D	
		Num fr. [*Hz*]	Δ (%)	Num fr. [*Hz*]	Δ (%)	Num fr. [*Hz*]	Δ (%)
1	4.645	4.616	0.628	4.529	2.561	4.561	1.842
2	9.128	9.096	0.352	8.955	1.932	9.127	0.011
3	11.447	11.309	1.220	12.052	-5.020	12.142	-5.724
4	14.481	14.508	-0.186	13.825	4.745	13.422	7.890

Table 7. Comparison between numerical and experimental modes through the MAC

	Model 1				Model 2				Model 3			
1_{exp}	0.988	0.001	0.000	0.001	0.988	0.001	0.000	0.003	0.988	0.000	0.006	0.002
2_{exp}	0.002	0.992	0.000	0.036	0.002	0.993	0.008	0.004	0.002	0.999	0.000	0.500
3_{exp}	0.023	0.000	0.909	0.000	0.028	0.000	0.906	0.002	0.022	0.000	0.947	0.000
4_{exp}	0.005	0.984	0.007	0.022	0.000	0.986	0.000	0.002	0.004	0.982	0.013	0.496
modes	1_{num}	2_{num}	3_{num}	4_{num}	1_{num}	2_{num}	3_{num}	4_{num}	1_{num}	2_{num}	3_{num}	4_{num}

In Table 7 has been reported a comparison between the experimental and numerical modes in terms of Modal Assurance Criterion (MAC, [34]). A good agreement for the first three modes has been observed (values very close to one) while a bad performance has been observed for the forth mode. In Table 8 the initial and updated values of Elastic modulus and Dead Load are reported. They are related to stiffness and mass, respectively, and so directly affect the modal frequencies. Regarding the elasticity modulus, a light decrease for all three models on average is about 5% is observed. Instead, more variability is found for the Dead Load but the final updated values are reasonable and limited between 1600 and 2000 N/m^2.

Table 8. Initial and updated (last step) parameters: elasticity modulus and dead load

Parameter	Model 1		Model 2		Model 3	
	Initial	Updated	Initial	Updated	Initial	Updated
Elasticity modulus [GPa]	195	191	205	197	193	190
Dead Load [N/m^2]	1900	1600	2000	1630	2000	2000

In Figure 15 the positions of the constrained nodes have been indicated. Six zones for models 2 and 3 have been selected (i.e. the positions from 1 to 6 in Figure 15a,b) at the ending elements. Instead, in model 1, the boundary conditions have been applied to three nodes from a side (nodes 2,3, and 4 in Figure 15c) and only one node on the other side (node 1 in Figure 15c). In Table 9 the releases of the DoFs for each constrained node and model, from initial to the final updated configuration has been illustrated.

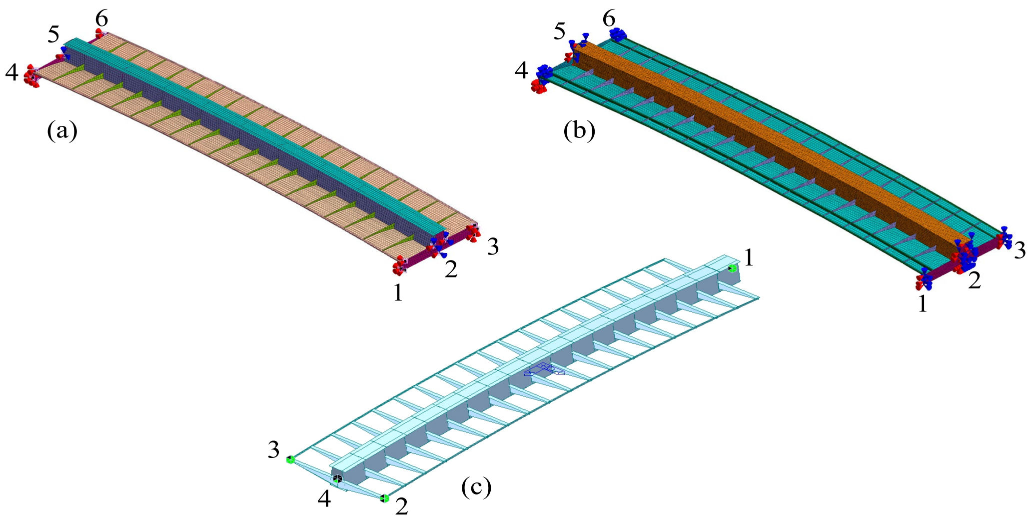

Figure 15. Highlights of the constrained supports for each model: 2D (a), 3D (b), and 1D (c)

The latter has been achieved by looking at the numerical modal shapes such that they are closer as much as possible to the identified one (Figure 10 and Figure 11). In Table 9 the values "1" and "0" mean DoFs fixed and free, respectively. Moreover, it is right to highlight the insertion of a linear spring in the vertical direction (Tz) with a stiffness of 9000 KN/m in position 4 of the model 1 (L.S. = Linear Spring in Table 9). This latter choice has been suggested by the realization of the support in position 4. In Figure 16 the first modes for each numerical model (in the columns) are illustrated. In each row, a comparison among the various models can be visualized (where "m" in Figure 16 means mode).

They are both in good agreement with each other and with the experimental modal shapes (Figure 10 and Figure 11). Especially, with the ones identified by the SSI procedure where a slight difference is found in the fourth mode (2nd torsional, probably due to a not correct identification on the phase).

5.3 Model Updating by Particle Swarm Optimization (PSO)

In this subsection, a method for solving the model updating using an optimization problem algorithm will be illustrated. Among various typologies found in the literature, PSO seems to be fast and simple to be implemented. Therefore, an algorithm for model updating of structure based on PSO optimization has been developed and tested for the case study, Annibaldi bridge.

5.3.1 PSO: origin and features

PSO method is a population-based approach developed by J. Kennedy J. and RC Eberhart R.C. [28]. The idea is to develop a particle swarm, moving within their parametric space, to find their target (minimization of the objective function). The method is very easy to be implemented, handled and executed with particular efficient in case of problems in which the target is finding the global solution. The single particle, in each iteration, has a memory of its previous best solution and also the ones of its neighbor. In the PSO, the displacement of the ith particle is defined by its position, x_i, and velocity, v_i, referred to the generic iteration. Position and velocity are determined through the following expressions:

$$x_i(k+1) = x_i(k) + v_i(k+1) \tag{2}$$

$$v_i(k+1) = v_i(k) + c_1 \cdot rand_1(0,1) \cdot \left(x_{best} - x_i(k)\right) + c_2 \cdot rand_2(0,1) \cdot \left(g_{best} - x_i(k)\right) \tag{3}$$

Eq. (2) defines the new position for each particle and iteration which is updated by the current position and its new velocity calculated using Eq. (3). The velocity is composed of different quantities:

1. current step velocity of the ith particle;
2. best previous position of the ith particle, x_{best};
3. the distance between the current position of the particle and the best one found by the

Table 9. Boundary conditions released for each numerical model from the initial to the updated configuration

model	Supports / DoF	Initial 1	Initial 2	Initial 3	Initial 4	Initial 5	Initial 6	Updated 1	Updated 2	Updated 3	Updated 4	Updated 5	Updated 6
1	Tx	1	1	1	1	-	-	1	1	1	0	-	-
	Ty	1	1	1	1	-	-	1	1	1	0	-	-
	Tz	1	1	1	1	-	-	1	1	1	0 + L.S.	-	-
	Rx	0	0	0	0	-	-	1	0	1	1	-	-
	Ry	0	0	0	0	-	-	0	1	1	0	-	-
	Rz	0	0	0	0	-	-	1	0	0	0	-	-
2	Tx	1	1	1	1	1	1	1	0	0	1	0	1
	Ty	1	1	1	1	1	1	1	1	1	1	1	1
	Tz	1	1	1	1	1	1	0	0	1	1	0	1
	Rx	1	1	1	1	1	1	0	1	0	0	1	0
	Ry	1	1	1	1	1	1	0	0	0	0	0	0
	Rz	1	1	1	1	1	1	0	1	0	0	1	0
3	Tx	1	1	1	1	1	1	0	0	0	1	0	1
	Ty	1	1	1	1	1	1	1	1	1	1	1	1
	Tz	1	1	1	1	1	1	0	0	0	1	0	1
	Rx	1	1	1	1	1	1	1	1	1	0	1	0
	Ry	1	1	1	1	1	1	0	0	0	0	0	0
	Rz	1	1	1	1	1	1	1	1	1	0	1	0

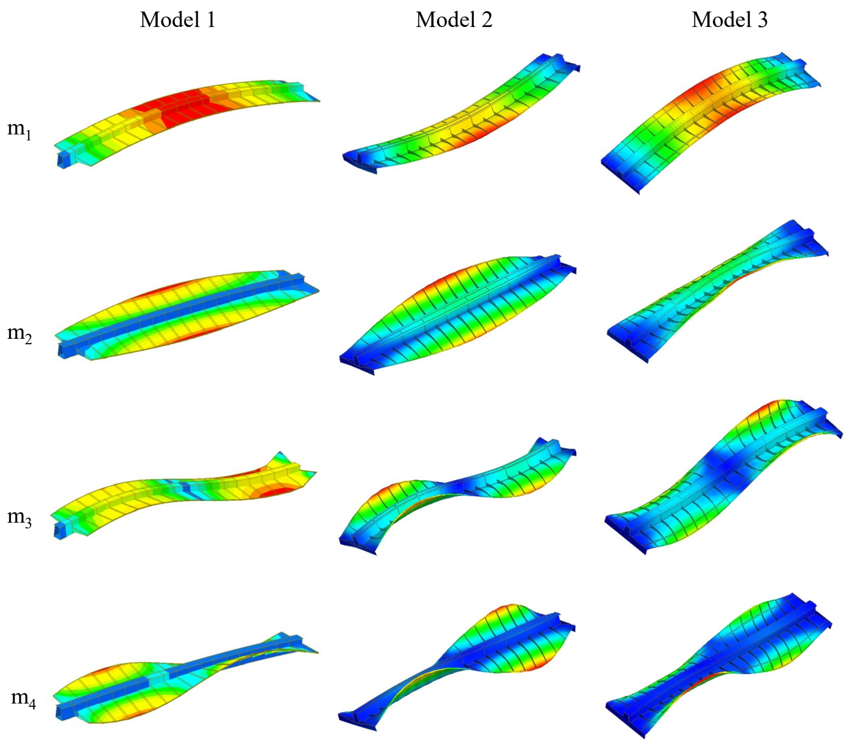

Figure 16: First four modal shapes of the updated models: 1D, 2D, and 3D (last step configuration). m = mode.

other particles of the swarm, g_{best} or global best.

The second and third terms are the so-called cognitive and social components, respectively, regulated by corresponding coefficients c_1 and c_2. The random coefficient $rand_1(0,1)$ and $rand_2(0,1)$ are uniformly distributed in the range [0,1]. The iterations will be stopped when the objective function will be minimized under a well-defined threshold or after a fixed number of iterations. Over the years, different variants have been applied to the PSO [35], one of which has been introduced by Clerc M. and Kennedy J. [36]. In their work, the authors introduce a constriction factor, χ, on the expression related to the velocity

which ensures convergence and improves the convergence rate. The new formula, Eq. (4) assumes the following form:

$$v_i(k+1) = \chi \cdot \left(v_i(k) + \phi_1 \cdot rand_1(0,1) \cdot \left(x_{best} - x_i(k)\right) + \phi_2 \cdot rand_2(0,1) \cdot \left(g_{best} - x_i(k)\right)\right) \quad (4)$$

The constriction coefficient is calculated as follows:

$$\chi = \frac{2}{\left|2-\phi+\sqrt{\phi^2-4\phi}\right|} \quad (5)$$

where $\phi = \phi_1 + \phi_2 > 4$. In the last formula ϕ_1 and ϕ_2 are random positive numbers drawn from a uniform distribution and defined by an upper limit.

The general procedure of the PSO algorithm has shown in the following Figure 17. In such figure *nPop* is the population size, while x_{best} and g_{best} are the best previous position of the ith particle and the global best position, respectively.

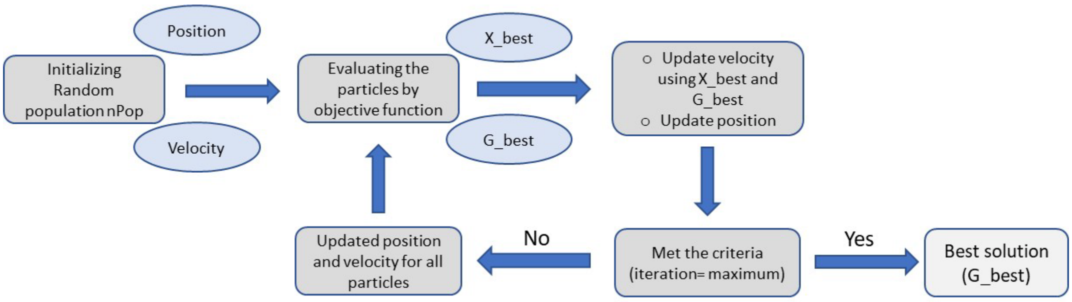

Figure 17. A general scheme of the PSO algorithm

5.3.2 Model updating by PSO and random elements

In this study, the proposed algorithm modifies the stiffness ($\mathbf{K_e}$) and mass ($\mathbf{M_e}$) matrices of each structural element directly using correction factors which are the variables of the optimization process. The case study of the Annibaldi pedestrian bridge has been modeled by transferring data from BIM to Matlab. FE analysis to obtain the modal parameters of the structure has been done by 1D elements in a 3D space. Using this element, a general beam that represents three translational and three rotational DoFs has been obtained. For this reason, a 3D finite element model has been implemented using Matlab by frame elements (6 DoFs for each node). As is shown in Figure 18, the algorithm uses text or excel data, coming from the BIM model, as input to form the FE model. From Dynamo Revit [37], such data can be extracted and saved in various formats (in this case have been saved in Excel format). The modal frequencies and shapes have been evaluated solving the eigenvalues problem:

$$\mathbf{Kx} = \omega_i^2 \mathbf{Mx} \qquad (6)$$

where $\mathbf{K}$ and $\mathbf{M}$ are the global stiffness and mass matrices, respectively, while the vector $\mathbf{x}$ contains all free DoFs in the global system. The value of the ith natural frequency is given by ω_i (ith eigenvalue) while the modal shapes will be the corresponding eigenvectors.

Two variables τ and θ will be considered in the application of the PSO algorithm. These coefficients will affect the stiffness and mass matrices, respectively, in some elements chosen randomly, in each iteration. This means that for a certain number of elements the stiffness matrix will be corrected by the aforementioned factors, while for other ones (some elements may be in common) the mass matrix will be modified. Two objective functions (OF), F_1 and F_2, applied in the updating process, have been defined as follows:

$$F_1 = \sum_{i=1}^{n} w_{i\omega} \left(\frac{f_i^{exp} - f_i^{num}}{f_i^{num}} \right)^2 \qquad (7)$$

$$F_2 = \sum_{i=1}^{n} w_{i\omega} \left(\frac{f_i^{exp} - f_i^{num}}{f_i^{num}} \right)^2 + \\ + w_m \sum_{i=1}^{n} \left(1 - diag\left(\mathrm{MAC}(\Phi_i^{exp}, \Phi_i^{num})\right) \right) \qquad (8)$$

where $w_{i\omega}$ and w_m are weight coefficients given by the following expressions:

$$w_{i\omega} = \frac{1}{f_i^{exp}} \qquad w_m = 1 \qquad (8)$$

Instead, Φ_i^{exp} and Φ_i^{num} denotes the modal vectors for the ith mode while n is the number of modes considered in the sum.

The algorithm aims to reduce, as much as possible, the difference between experimental and numerical frequencies. For this reason, the particles represent the elements of two sets of random vectors, one set for the stiffness and the other one for the mass. The fundamental steps of the procedure can be defined as follow:

1. Selection of a random number, R_K and R_M, respectively for stiffness and mass: $R_K \in [1, N_e]$ (stiffness) and $R_M \in [1, N_e]$ (mass). Where N_e is the total elements number.
2. Generation of two set random vectors for stiffness and mass, with the dimension

driven by the previous coefficients (R_K and R_M): $\boldsymbol{R_K}$ and $\boldsymbol{R_M}$. The elements of these two sets of vectors will be selected randomly within the range between 1 and N_e. Each number will be corresponding to a single structural element in the numerical model. The random numbers will be such that they are not duplicated and listed in decreasing or increasing order.

The procedure of model updating using the modified particle swarm optimization has been illustrated in the flowchart reported in Figure 18. The procedure aims to the automatic transformation of data from BIM to form a FE model and its subsequently updating by PSO optimization. The improvement of structural elements will be done by modifying the stiffness and mass matrices of the elements. The uncertainty limits of the parameters can define the search space of the correction factors. In the mass matrix, the density of the material, the length of the element, and the section properties are determining parameters and for most cases (like this case study), the geometry can be considered a parameter certain (especially when using BIM data) while the only uncertainty could be related to the density. However, the density of the material (steel) is usually provided by the manufacturer, but for modal analysis, the dead loads also are considered as a part of the mass of the structure. Therefore, such loads here are uncertain but limited by upper and lower values used to form a search space for mass matrix correction factor. On the other hand, for the stiffness matrix beside the geometry which is also considered certain, the elasticity modulus is the target to be pursued. It should be noticed that the search space could differ by the condition of the problem and the structure that could lead to the definition of more appropriate variables in the optimization problem.

As mentioned before, in this case, the uncertainties have been boundary conditions, elasticity modulus, and loads. However, for initializing the algorithm, the boundary conditions, since have been updated in the previous section, have been considered as a certain parameter. Therefore, the correction procedure will not influence the boundary conditions where 0 and 1 are considered as free and restrained DoF, respectively. It should be noticed that using this algorithm and with some modification, also different possible boundary

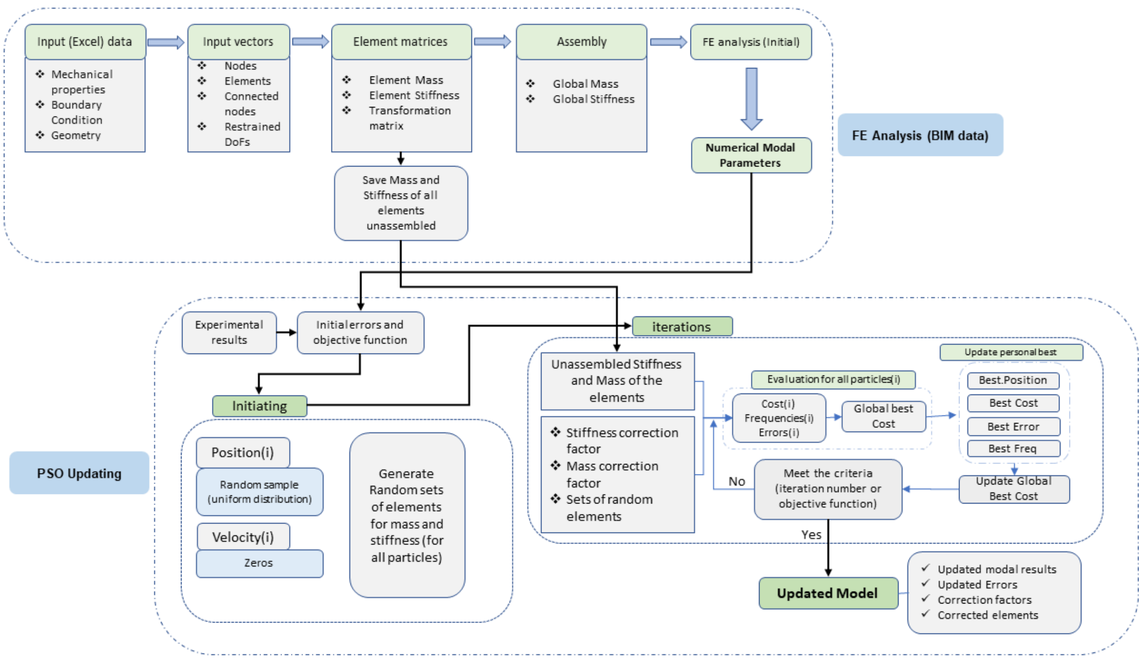

Figure 18. Model updating process using BIM data and modified PSO optimization (random elements correction)

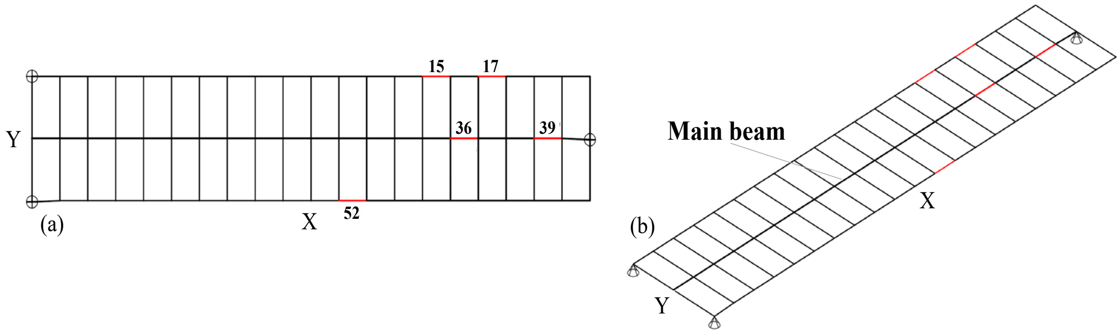

Figure 19. Numerical model implemented in Matlab: (a) plane and (b) 3D view. In red: example of random elements selected for the PSO procedure.

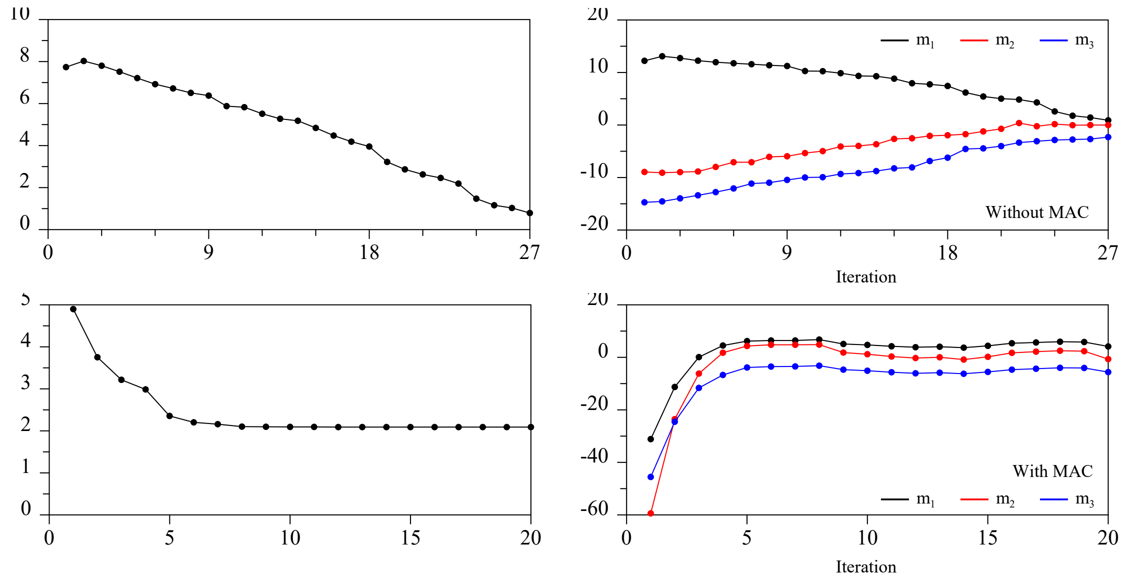

Figure 20: Trend of the Objective Functions considered for the process of model updating and corresponding errors between numerical and experimental modes: without (a),(b) and with (c),(d) MAC. m = mode.

conditions could be considered, for specific nodes, enlarging the search space.

In the numerical simulations, the initial values of the model are as follow: elasticity modulus 2.00e+11 [N/m^2], Poisson coefficient 0.3 [-], shear modulus 7.69e+10 [N/m^2], dead load 2000 [N/m^2]. In Figure 19 a sketch of the model in Matlab is illustrated. In this representation, some random elements, highlighted in red color, represent the elements considered for the correction of the stiffness matrix. In Figure 20a the behavior of the first OF, F_1, in each step of the procedure is illustrated. It shows how each value aims to go toward the optimal solution. In Figure 20b the corresponding trends of the percentage errors for the first three modes are reported. Also, in this case, a clear and reasonable choice of the parameters τ and θ to reach the target very quickly is evident. Instead, in the Figure 20c and Figure 20d are illustrated the behaviour of the second OF F_2 and the corresponding trends of the percentage errors for the first three modes. In this second procedure the average percentage error is noticeably higher. Indeed, looking to the results reported in Table 10 the average error is of 1.058% and 10.101% applying, respectively the first and second. Instead, in Table 11 have been highlighted the results in terms of MAC showing a scenario comparable. Indeed, three of the four values in the main diagonals are near and over 0.9 for while the almost all terms out diagonal are very close to zero. This behaviour has been obtained using both OFs. However, the easaly in the execution and

Table 10: Results of the model updating by PSO applied to random elements in terms of frequencies

Modes	Exp. Freq. [Hz]	Objective function F_1		Objective function F_2	
		Num. Freq. [Hz]	Δ (%)	Num. Freq. [Hz]	Δ (%)
1	4.645	4.604	0.887	4.461	4.134
2	9.128	9.129	-0.007	7.627	19.674
3	11.447	11.714	-2.280	12.127	-5.608

Table 11: Results of the model updating by PSO applied to random elements in terms of MAC

	Objective function F_1				Objective function F_2			
1_{exp}	0.975	0.003	0.006	0.001	0.976	0.003	0.008	0.000
2_{exp}	0.002	0.004	0.000	0.936	0.002	0.105	0.000	0.706
3_{exp}	0.028	0.000	0.961	0.000	0.028	0.000	0.966	0.000
4_{exp}	0.005	0.001	0.009	0.893	0.005	0.001	0.008	0.901
modes	1_{num}	2_{num}	3_{num}	4_{num}	1_{num}	2_{num}	3_{num}	4_{num}

manage of the procedure leads to some drawbaks: (1) the difference percentage between the forth experimental and numerical mode is very high for both OFs (about 33% and -18% respectively for the first and second OF), (2) the first and third modal shape (symmetric and antisymmetric flexural, respectively, illustrated in Figure 21a,) are in good agreement with the experimental ones but the second one shows an antisymmetric torsional shape (Figure 21b).

In any way, considering the easiness of implementation and quickness of the algorithm, the results could be assumed reasonable. The final values of τ and θ are reported in the following Table 12. Looking ot the results is evident an higher forcing of the nominal parameters for the second OF (F_2).

Table 12: Results of the model updating by PSO applied to random elements in terms of MAC

OF	τ	θ
F_1	0.94	1.13
F_2	0.75	1.31

6. Discussion and conclusions

The study describes a procedure of model updating related to a bridge structure using geometric and information data derived by a BIM model and mechanical data tuned based on vibration measurements. The model updating has been pursued by two approaches: manual and automatic. BIM can provide a highly detailed model of the facility or building in terms of geometry and material or other corresponding properties. This model contains a trustful and rich data source that can be used by different experts and users operating in the design or life-cycle management fields of a building. However, especially from the point of view of structural analysis, there are huge amount of unnecessary data and information depending on the type of analysis. For instance, the geometrical details useful to carry out a linear dynamic analysis (e.g. modal analysis) are typically different from the ones that should be modeled to perform a nonlinear static analysis (e.g. refined model to follow the damage propagation). In this latter case, a cost-benefit analysis is opportune to understand the level of modeling refinement. For this reason, in this study, three different models representative of the dynamic behavior of the pedestrian walkaway using three different levels of discretization have been implemented. Such models have been realized by selecting different types of elements. In particular, in the first model (model 1) beam elements have been predominantly chosen while for the second and third models (models 2 and 3) 2D (shell) and 3D (solid) elements have been applied, respectively. A manual model updating of these three models, aiming to reduce the distance of the experimentally identified frequencies from the numerical ones, has been pursued. The following observations can be mentioned:

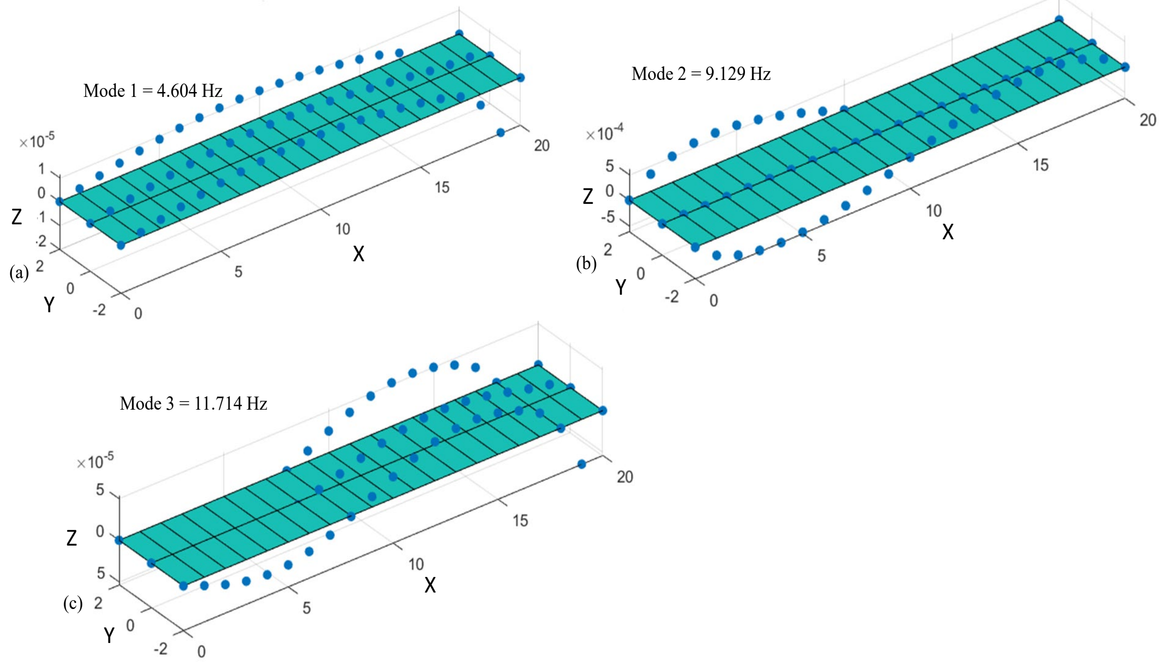

Figure 21: Numerical modes updated by PSO procedure applied to random elements.

1. if from one side model 1 needs more geometric approximations and idealization, from the other side a smaller number of DoFs helps to achieve the minimum difference between numerical and experimental frequencies.
2. The interoperability of BIM and FEA is an efficient solution for structural analysis and model updating. This can lead to reaching more accurate and powerful approaches for structural design and health monitoring. Here, two methods of transferring data have been tested also for investigating the effective automatization of the whole procedure. For this bridge, with mostly curved form members, the geometry modelling has been simplified.
3. The models 2 and 3 show a high analysis computational time compared to the model 1 (20 and 30 times higher) due to the need of using a large number of DoFs. The manual model updating for models 2 and 3 has not achieved the same performance obtained for model 1 but, at the same time, such models permit a better description of the tensional and deformative state.
4. Such assessments have been drawn only considering a single case study. Other situations should be analyzed to delineate a statistical outline.

The manual model updating illustrated is sometimes a process that can be very cumbersome. For example, the perceptibility in identifying the parameters more sensitive is surely the first step to be evaluated accurately. Moreover, also the subsequent parametric analysis is a procedure very heavy to be implemented. For these reasons, in the last part of the paper, a modified PSO has been developed to check the performance provided by a possible procedure of automatic model updating. The application showed promising results, but it should be applied by analyzing other structural typologies.
This activity could be considered as a first tentative in the investigation of the possibilities related to the interoperability between structural

`

modelling and data and information coming from BIM and experimental dynamic tests. A simple and preliminary automatic procedure has been developed with the aim of both speeding up the process and addressing the implementation of a digital twin of the bridge under investigation.

Acknowledgments: Part of the research leading to these results has received funding from the Italian Government under Cipe resolution n.135 (Dec. 21. 2012) under the project INCIPICT-INnovating City Planning through Information and Communication Technologies. The experimental results of the Annibaldi walkway are part of the research project DESDEMONA - DEtection of Steel Defects by Enhanced MONitoring and Automated procedure for self-inspection and maintenance (grant agreement number RFCS-2018_800687) supported by EU Call RFCS-2017. This research was in part sponsored by the NATO Science for Peace and Security Programme under grant id. G5924.

Data Availability Statement: Some or all data, models, or codes that support the findings of this study are available from the corresponding author upon reasonable request.

Conflicts of Interest: The authors declare no conflicts of interest.

References

1. Foti D, Gattulli V, Potenza F (2014) Output-Only Identification and Model Updating by Dynamic Testing in Unfavorable Conditions of a Seismically Damaged Building. Comput. Aided Civil Infrastruct Eng 29(9):659-675.
2. Gattulli V, Cunha A, Caetano E, Potenza F, Arena A, Di Sabatino U (2021) Dynamical models of a suspension bridge driven by vibration data. Smart Struct. Syst. 27(2):139-156.
3. Gattulli V, Lepidi M, Potenza F, Di Sabatino U (2016) Dynamics of masonry walls connected by a vibrating cable in a historic structure. Meccanica 51(11):2813-2826.
4. Gattulli V, Lepidi M, Potenza F, Di Sabatino U (2019) Modal interactions in the nonlinear dynamics of a Beam-Cable-Beam. Nonlinear Dynamics 96(4):2547-2566.
5. Gattulli V, Lofrano E, Paolone A, Potenza F (2019) Measured properties of structural damping in railway bridges. J. Civ. Struct. Heal. Monit. 9(5):639-653.
6. Lepidi M, Gattulli V, Vestroni F (2009) Damage Identification in Elastic Suspended Cables through Frequency Measurement. J. Vib. Control 15(6):867-896.
7. Masciotta MG, Pellegrini D, Brigante D, Barontini A, Lourenco PB, Girardi M, Padovani C, Fabbrocino G (2019) Dynamic characterization of progressively damaged segmental masonry arches with one settled support: experimental and numerical analyses. Frat. ed Integrità Strutt. 14(51):423-441.
8. Domaneschi M, Zamani Noori A, Pietropinto MV, Cimellaro GP (2021) Seismic vulnerability assessment of existing school buildings. Comput. Struct. 248:106522.
9. Fayyadh MM, Razak HA (2022) Experimental assessment of dynamic and static based stiffness indices for RC structures. Structures, 45:459-474.
10. Peeters B, De Roeck G (2000) Reference based stochastic subspace identification in Civil Engineering. Inverse Probl. Eng. 8(1):47-74.
11. Peeters B, Van der Auweraer H (2005) PolyMAX: A revolution in operational modal analysis. In: Proc. 1st Int. Oper. Modal Anal. Conf. IOMAC 2005, 26-27 April, Copenhagen, Denmark.
12. Pasca DP, Aloisio A, Rosso MM, Sotiropoulos (2022) PyOMA and PyOMA_GUI: A Python module and software for Operational Modal Analysis. SoftwareX, 20, 101216.
13. Giordano PF, Ubertini F, Cavalagli N, Kita A, Masciotta MG (2020) Four years of structural health monitoring of the San Pietro bell tower in Perugia, Italy: two years before the earthquake versus two years after. Int. J. Mason. Res. Innov. 5(4):445-467.
14. Di Girolamo GD, Smarra F, Gattulli V, Potenza F, Graziosi F, D'Innocenzo A (2020) Data-driven optimal predictive control of seismic induced vibrations in frame structures. Struct. Control Heal. Monit. 27(4):e2514.
15. Dallard PRB, Fitzpatrick AJ, Flint A (2001) The London Millennium Footbridge. Struct. Eng. 79:17–33.
16. Zivanovic S, Pavic A, Reynolds P (2006) Modal testing and FE model tuning of a lively footbridge structure. Eng. Strcut. 28:857-868.

`

17. Van Nimmen K, Lombaert G, De Roeck G, Van den Broeck P (2014) Vibration serviceability of footbridges: Evaluation of the current codes of practice. Eng. Struct. 59:448-461.
18. Lai E, Gentile C, Mulas MG (2017) Experimental and numerical serviceability assessment of a steel suspension footbridge. J. Constr. Steel Res. 132:16-28.
19. Banas A, Jankowski R (2020) “Experimental and Numerical Study on Dynamics of Two Footbridges with Different Shapes of Girders. Applied Sciences 10(13):4505.
20. Caetano E, Cunha Á, Moutinho C, Magalhães F (2010) Studies for controlling human-induced vibration of the Pedro e Inês footbridge, Portugal. Part 2: Implementation of tuned mass dampers. Eng. Struct. 32(4):1082-1091.
21. Caetano E, Cunha Á, Magalhães F, Moutinho C (2010) Studies for controlling human-induced vibration of the Pedro e Inês footbridge, Portugal. Part 1: Assessment of dynamic behaviour. Eng. Struct. 32(4):1069-1081.
22. Drygala IJ, Polak MA, Dulinska JM (2019) Vibration serviceability assessment of GFRP pedestrian bridges. Eng. Struct. 184:176-185.
23. Hu WH, Caetano E, Cunha A (2013) Structural health monitoring of a stress-ribbon footbridge. Eng. Struct. 57:578-593.
24. Singh P, Sadhu A (2020) System Identification-Enhanced Visualization Tool for Infrastructure Monitoring and Maintenance. Front. Built Environ., 6.
25. Garbett J, Hartley T, Heesom D (2021) A multi-user collaborative BIM-AR system to support design and construction. Autom. Constr. 122:103487.
26. Sattler L, Lamouri S, Pellerin R, Maigne T (2019) Interoperability aims in Building Information Modeling exchanges: a literature review. IFAC-PapersOnLine 52(13):271-276.
27. O’Shea M, Murphy J (2020) Design of a BIM integrated structural health monitoring system for a historic offshore lighthouse. Buildings 10(7):131.
28. Eberhart R, Kennedy J (1995) A New Optimizer Using Particle Swarm Theory. In: Proceedings of the Sixth International Symposium on Micro Machine and Human Science, 4-6 October, Nagoya, Japan.
29. Aloisio A, Pasca DP, Di Battista L, Rosso MM, Cucuzza R, Marano GC, Alaggio R (2022) Indirect assessment of concrete resistence from FE model updating and Young's modulus estimation of a multi-span PSC viaduct: experimental tests and validation. Strutures 37:686-697.
30. Demartino C, Quaranta G, Maruccio C, Pakreshi V (2022) Feasibility of energy harvesting from vertical pedestrian-induced vibration of footbridges for smart monitoring applications. Computer-Aided Civil and Infrastructure Engineering 37(8) 1044-1065.
31. Rosso MM, Cucuzza R, Aloisio A, Marano GC (2022) Enahnced Multi-Strategy Particle Swarm Optimization for Constrained Problems with an Evolutionary-Strategies-Based Unfeasible Local Search Operator. Applied Sciences 12(5) 2285.
32. Reynders E, Schevenels M, De Roeck G (2014) MACEC 3.3 A Matlab toolbox for experimental and operational modal analysis. Faculty of Engineering, Department of Civil Engineering, Structural Mechanics Section, Kasteelpark Arenberg 40, B-3001 Leuven.
33. Siemens Digital Industries Software, Simcenter TestLab (https://www.plm.automation.siemens.com/global/it/products/simcenter/testlab.html).
34. Allemang R (2003) The modal assurance criterion - Twenty years of use and abuse. J. Sound Vib. 37(8):14-23.
35. Wang D, Tan D, Liu L (2018) Particle swarm optimization algorithm: an overview. Soft Comput. 22(2):387-408.
36. Clerc M, Kennedy J (2002) The particle swarm-explosion, stability, and convergence in a multidimensional complex space. IEEE Trans. Evol. Comput., 6(1):58-73.
37. Dynamo BIM. 2017. “Dynamo BIM–Community-driven open source graphical programming for design.” Accessed February 10, 2017. http://dynamobim.org.